Ocean Sci. Discuss., 10, 1099–1125, 2013
www.ocean-sci-discuss.net/10/1099/2013/
doi:10.5194/osd-10-1099-2013

Ocean Science
Discussions
Open Access

Turbulent dispersion properties from a model simulation of the western Mediterranean

H. Nefzi[1], **D. Elhmaidi**[1], **and X. Carton**[2]

[1]Faculté des Sciences de Tunis –Université Tunis Elmanar, Tunisie
[2]Laboratoire de Physique des Océans-Université Occidentale de Bretagne Brest, France

Received: 7 June 2013 – Accepted: 11 June 2013 – Published: 10 July 2013

Correspondence to: D. Elhmaidi (dalila.elhmaidi@fst.rnu.tn)

Published by Copernicus Publications on behalf of the European Geosciences Union.

Abstract

Using a high resolution primitive equation model of the western Mediterranean Sea, we analyzed the dispersion properties of a set of homogeneously distributed, passive particle pairs. These particles were initially separated by different distances D_0 (D_0 = 5.55, 11.1 and 16.5 km), and were seeded in the model at initial depths of 44 and 500 m.

This realistic ocean model, which reproduces the main features of the regional circulation, puts in evidence the three well-known regimes of relative dispersion.

The first regime due to the chaotic advection at small scales, lasts only a few days (3 days at 44 m depth, a duration comparable with the integral time scale) and the relative dispersion is then exponential. In the second regime, extending from 3 to 20 days, the relative dispersion has a power law t^{α} where α tends to 3 as D_0 becomes small. In the third regime, a linear growth of the relative dispersion is observed starting from the twentieth day. For the relative diffusivity, the D^2 growth is followed by the Richardson regime $D^{4/3}$. At large scales, where particle velocities are decorrelated, the relative diffusivity is constant.

At 500 m depth, the integral time scale increases (> 4 days) and the intermediate regime becomes narrower than that at 44 m depth due to weaker effect of vortices (this effect decreases with depth). The turbulent properties become less intermittent and more homogeneous and the Richardson law takes place.

1 Introduction

The ocean currents carry heat, salt, momentum, nutrients, and pollutants. Some of these transport processes are at the heart of the mechanism of climate variability and of marine ecosystem functioning. In addition, many available data on ocean dynamics come from float and drifter trajectories and measurements. Therefore, the knowledge of transport and dispersion processes in the ocean is essential.

OSD
10, 1099–1125, 2013

Satellite observations and numerical models of the western Mediterranean Basin have revealed the presence of coherent vortices generated by the instability of the inflowing Atlantic water through the Gibraltar strait. Such vortices can survive for long durations, carrying waters of their origin and playing an essential role in transport and mixing processes. (Millot, 1999; Millot et al., 2005). On the other hand, numerical experiments of two-dimensional turbulence have shown that the presence of vortices induces an anomalous intermediate dispersion regime between the ballistic regime and the Brownian one. The study of the absolute dispersion of neutral floats in two-dimensional flows and in the western Mediterranean Basin has revealed that the absolute dispersion anomalous regime is characterized by a power law t^r where r varies between 5/3 and 5/4 (Elhmaidi et al., 1993, 2010). The corresponding intermediate regime for the relative dispersion is known as the Richardson regime (Richardson, 1926; Babiano et al., 1990).

Many analyses of oceanic data have shown the existence of the Richardson regime (LaCasce and Bower, 2000; LaCasce and Ohlmann, 2003; Ollitraut et al., 2005; Lumpkin and Elipot, 2010). Such oceanic data were obtained using subsurface or surface drifters. Nevertheless, though large, the number of float or drifter data in the world ocean remains small compared to the ocean surface (or volume) so that their average separation is relatively large and that they do not provide a uniform coverage of the ocean. The use of synthetic drifters in numerical simulations can palliate this deficiency and help test the accordance between numerical and experimental data. Usually, particle tracking in numerical models was used to follow the path or mixing of water masses. Here we aim to put in evidence the theoretical regimes of turbulent dispersion in the marine dynamics context.

In the present work, we study the dispersion of passive particle pairs, near the surface, in the western Mediterranean Sea. We use a high resolution model of this half-basin able to reproduce a realistic level of turbulence (mesoscale eddies). In Sect. 2, we recall the numerical conditions of the study (the model and its parameters). In Sect. 3, we briefly recall the theoretical results of turbulent dispersion in quasi-2-D flows. Sec-

OSD
10, 1099–1125, 2013

tion 4 is devoted to the analysis of the model results and to the calculation of dispersion and of relative diffusivity. Finally conclusions are drawn.

2 The ROMS model

The Regional Ocean Modeling System (ROMS) is a primitive equation model able to simulate both coastal and oceanic regions. It is based on the Boussinesq approximation and on the hydrostatic balance. ROMS is a split-explicit, free surface oceanic model discretised in coastline and terrain-following curvilinear coordinates. Short time-steps are used to solve the barotropic momentum equations and longer ones to advance the baroclinic momentum equations. A third-order, upstream-biased advection scheme implemented in ROMS allows the generation of steep gradients, enhancing the effective resolution of the solution for a given grid size (Shchepetkin and McWilliams, 2005; Penven et al., 2008). The explicit lateral viscosity is zero everywhere in the model domain except in the sponge layers near the boundaries where the viscosity increases smoothly toward the lateral open boundaries.

The computational domain for this study extends from 33° to 44.5° N and from 7° W to 15° E. The model grid, forcing, initial and boundary conditions are built using the ROMSTOOLS package (Shchepetkin and McWilliams, 2005; Penven et al., 2008). The bottom topography is derived from the 2' resolution database ETOPO2 (Penven et al., 2010). A slope parameter $r = 2.5$ is used to prevent errors in the computation of pressure gradient (Smith and Sandwell, 1997). The ROMS configuration used here has a 1/8° horizontal resolution and 20 vertical levels with stretched s-coordinates, using surface and bottom stretching parameters ($\theta_s = 0, \theta_b = 6$) (Haidvogel and al., 2000). Mean monthly temperature and salinity data are obtained from World Ocean Atlas (WOA, 2005) database (monthly climatology at $1° \times 1°$ resolution) (Song and Haidvogel, 1994).

Figure 1 represents the model grid and its bathymetry. At the two open boundaries (west and east), an active, implicit, upstream biased radiation condition connects the

OSD
10, 1099–1125, 2013

model solution to the surrounding sea or ocean (Conkright et al., 2001). The model is forced with winds, heat and salinity fluxes from the Comprehensive Ocean-Atmosphere Data Set (COADS05) which is a monthly climatology giving data with spatial resolution of 0.5° (Da Silva et al., 1994; Marchesiello et al., 2001). The width of the nudging border is 150 km and the maximum viscosity value for the sponge layer is set to 1000 $m^2 s^{-1}$.

We performed numerical simulations, with the ROMS model, to study the dispersion processes in the western Mediterranean Basin. We have shown in a previous paper that the surface currents simulated by the ROMS model are consistent with available in situ and satellite data sets (Elhmaidi et al., 2010). In particular, the ROMS model reproduced the large scale currents and the meso-scale eddies with the proper distribution of intensity and location.

In this model, we seeded neutral, passive particles. The Lagrangian velocities were calculated using a centred scheme; the interpolation scheme for the particle trajectories is a fourth-order accurate Adams–Bashford–Moulton predictor-corrector scheme. Transport of particles was due to advection only, as no diffusion term was introduced.

3 Relative dispersion

To study particle dispersion, relative dispersion and relative diffusivity are used (Richardson, 1926; Babiano et al., 1990). They are related to the turbulent cascade process in the Eulerian velocity field. They are defined respectively by:

$$D^2(t, D_0) = \sum_{i \neq j} (\boldsymbol{x}_i(t, D_0) - \boldsymbol{x}_j(t, D_0))^2 \quad (1)$$

$$Y(t) = \frac{1}{2} \frac{d}{dt} D^2(t, D_0) \quad (2)$$

where $\boldsymbol{x}_i$(t,D_0) and $\boldsymbol{x}_j(t, D_0)$ are the particle positions of a pair separated initially by D_0.

In 3-D isotropic homogeneous and stationary flows, where the energy spectrum has the form $E(k) \approx k^{-5/3}$, (where k is the wave number), the asymptotic regime of the

OSD
10, 1099–1125, 2013

relative dispersion and the relative diffusivity can be obtained by the Richardson laws (Babiano et al., 1990):

$$D^2(t, D_0) \approx t^3, Y(t) \approx D^{4/3}(t).$$

In 2-D homogenous isotropic turbulence, the flow is characterized by two inertial ranges: the range of enstrophy cascade and the range of inverse energy cascade, for which the energy spectra are respectively: $E(k) \approx k^{-3}$ and $E(k) \approx k^{-5/3}$.

The following Richardson's and Lin's laws for the relative dispersion of two-dimensional turbulence are a t^3 law in the inverse energy range and an exponential evolution in the enstrophy cascade range (Babiano et al., 1990).

The relative diffusivity has also two shapes: $Y(t) \approx D^2(t)$ in the enstrophy cascade range, and $Y(t) \approx D^{4/3}(t)$ in the inverse energy range.

At larger separation distances, relative dispersion is a random walk and relative diffusivity is constant.

After a sufficiently long time, the separation distance of the particle pair reaches the scale of the energetic eddies and the velocities of the two particles decorrelate. Due to homogeneity, the zonal mean-square relative velocity becomes just four times the eddy kinetic energy (LaCasce and Bower, 2000):

$$\left\langle \left(\frac{d\boldsymbol{D_x}}{dt} \right)^2 \right\rangle = \langle (\delta u)^2(t, D_0) \rangle = \langle u_i^2 \rangle + \langle u_j^2 \rangle - 2\langle \boldsymbol{u_i} u_j \rangle \approx 2\langle \boldsymbol{u_i^2} \rangle$$

where $\boldsymbol{u_i}$ and $\boldsymbol{u_j}$ are the individual zonal velocities of the particle pair (note that the diagnostics on zonal, meridional and isotropic components are identical for this model of turbulence in the Mediterranean Sea).

At early times, the individual particle velocities are correlated and the zonal mean-square relative velocity tends toward $Z D_0^2$ where Z is the enstrophy defined by (Babiano et al., 1990; Ollitrault et al., 2005).

OSD
10, 1099–1125, 2013

The enstrophy can be calculated through the relative dispersion characteristic time defined by:

$$\tau(D) = \frac{D^2}{Y(t)} \quad ,$$

which is constant, and tends toward $\frac{2}{Z^{1/2}}$ when D tends to zero, and which has a power law $\tau(D) \approx D^{2/3}$ in the inverse energy cascade range (Babiano et al., 1990).

4 Results

2726 passive particles pairs were homogeneously seeded at subsurface ($h = -44$ m) of the model for different separation distances D_0. Note that the results presented hereafter were independent of this initial depth as long as the particles were seeded in the turbulent surface layer (from zero to −100 m). Particles remained at the same depth for the whole duration of the simulations. The particle initial positions were identical for all the simulations. Their initial positions were located between 36° and 39° N in latitude and 0° and 12° E in longitude. They were advected with the interpolated model velocity during two months. The float positions, for $D_0 = 5.55$ km, are shown on Fig. 2 at the end of the simulation. In the inset, we show the initial particle positions. The particles travel to the East in accordance with the main circulation. They disperse in the whole domain and some of them aggregate around vortices in energetic domains. This particle evolution is similar to that in two-dimensional turbulence where vortices constitute a barrier transport, trap passive floats and induce a far field effect (Elhmaidi et al., 1993, 2005).

The temporal evolution of the mean square relative zonal velocity (δu^2) and four times the zonal kinetic energy (4E) are plotted for the value $D_0 = 5.55$ km on Fig. 3a. This evolution can be described in three different phases.

In the first one (the first ten days), the energy firstly remains nearly constant for about three days, as the Lagrangian velocities are correlated. This time interval is roughly

OSD
10, 1099–1125, 2013

equal to the Lagrangian integral timescale defined by

$$T_L = \int_0^\infty R(\tau) d\tau$$

where

$$R(\tau) = \frac{\langle \boldsymbol{u}(t).\boldsymbol{u}(t+\tau) \rangle}{\langle \boldsymbol{u}(t).\boldsymbol{u}(t) \rangle}$$

is the Lagrangian velocity autocorrelation displayed on Fig. 3b. Then (until about day 20), the energy increases because the particles are trapped in the intense circulation cells around vortices. During this phase, the mean square relative velocity has a quasi-linear evolution.

In the second phase (days 10 to 30), the decrease of the energy is marked and the mean square relative velocity is close to constant.

In the final phase ($t > 30$ days), the evolutions of 4E and δu^2 are correlated and the mean square relative velocity roughly equilibrates to four times the kinetic energy with a 0.05 difference.

The mean square relative velocity for the different separation distances is displayed on Fig. 3c. Between days 2 and 10, δu^2 has a power law t^b where b is roughly equal to one (Babiano et al., 1990).

When t is small, δu^2 tends to ZD_0^2, while the enstrophy Z fluctuates between 0.44 and 1.2 day s^{-2}.

On Fig. 4a, the temporal evolution of the zonal relative dispersion is plotted for different pair separation distances (D_0 = 5.55, 11.1 and 16.6 km). This evolution can be described in three phases.

The first one lasts three days. In the second phase, Fig. 4a seems to indicate that D^2 grows like t^a where a varies between 1.6 and 3. For small initial separations D_0, the

OSD
10, 1099–1125, 2013

exponent a tends to three. In the third phase, a linear growth of the relative dispersion is observed starting from the twentieth day.

To analyse the temporal evolution of the relative dispersion in the first phase, D^2 is displayed in a log-linear plot on Fig. 4b.

A linear evolution is first observed for the different value of D_0. This is an indication of the exponential growth while the dispersion is dominated by eddies with scales larger than the pair separations. This regime is present for $D_0 = 5.55$ km and 11.1 km. Then $D^2(t, D_0) \approx \exp(kt)$, where k varies between 0.74 and 0.82. This exponential regime was found previously for separation distances smaller than the Rossby radius of deformation (LaCasce and Bower, 2000; LaCasce and Ohlmann, 2003; Ollitraut et al., 2005; Lumpkin and Elipot, 2010).

The relative dispersion coefficient $Y(D)$ was calculated by finite time differencing $D^2(t, D_0)$. Its evolution versus D, compensated by D^2 and $D^{4/3}$, is shown on Fig. 5a, b for several initial distances D_0 ($D_0 = 5.55$, 11.1 and 16.6 km). For $D_0 = 5.55$ or 11.1 km, the $Y(D) \approx D^2$ regime is present for the small scale range as seen on Fig. 5a. The plateau extends from 6 to 10 km for the smallest D_0. For $D_0 = 16.6$ km, there is no plateau. The D^2 regime confirms the presence of an enstrophy cascade range only for an initial distance D_0 smaller than about 11 km. The Richardson $D^{4/3}$ regime is visible on Fig. 5b for the different initial distances. It extends from 11 to 55 km.

The enstrophy Z of the flow can be calculated via the evolution of the relative characteristic dispersion time reported on Fig. 6a. For small D, the minimum characteristic time is about 2 days and the corresponding enstrophy value $Z \approx 1\,\text{day}^{-2}$. This value is in the range of the enstrophy calculated with the minimum of the square relative velocity. The Richardson regime $D^{2/3}$ law in the inverse energy cascade range is manifested by the presence of a plateau on the plot of $\tau(D)$ compensated by $D^{-2/3}$ for the different initial separations (Fig. 6b).

OSD
10, 1099–1125, 2013

In a previous work we have shown that, at large depth, the intermediate absolute dispersion follows a power law over a period of time shorter than near the surface due to the weaker effect of vortices (this effect decreases with depth, Elhmaidi et al., 2010).

To verify this result for the relative dispersion, 833 pairs of particles are seeded at the 500 mdepth initially separated by the values of D_0 already used. The relative dispersion for the three values of D_0 is shown on Fig. 7. We can distinguish the presence of the three phases described above with a narrow intermediate phase. In effect, the temporal evolution of the surface and deep Lagrangian correlation functions (Fig. 8) shows that the surface particles velocities decorrelate more rapidly than the deep ones. Thus, the duration of the depth first phase is longer. The second phase in which the dispersion has a power law, extends from the 5th to the 15th day. For the lowest value of D_0, the relative dispersion reduced by t^{-3} (Fig. 9) shows the existence of a plateau that is the signature of the Richardson law. Given the weaker effect of vortices at depth, the turbulent properties become less intermittent and more homogeneous and the Richardson law takes place.

Our results are consistent with the analysis of the subsurface drifters released respectively in the Gulf Stream and in the North Atlantic Current at 700 m depth (LaCasce and Ohlmann, 2003; Ollitrault et al., 2005).

5 Conclusions

In this work, we have studied the relative dispersion of neutral passive particle pairs, separated by different initial distances D_0(D_0 = 5.55, 11.1 and 16.65 km), deployed in the western Mediterranean Sea at initial depths 44 and 500 m. The particles were advected with the ROMS model velocity interpolated over the particle trajectories.

The analysis of the model output has shown that the relative dispersion laws are similar to those of 2-D turbulence with the presence of the three well known regimes.

OSD
10, 1099–1125, 2013

The first regime characterizes the chaotic advection at small scales, lasts only a few days (3 days, a duration equivalent to the integral time scale), and the relative dispersion is exponential.

In the second regime, extending from 3 to 20 days, the relative dispersion follows a power law t^{α} where α tends to 3 for small D_0, according to the Richardson regime.

In the third phase, a linear growth of the relative dispersion is observed starting from the twentieth day.

The relative diffusivity has also three behaviours according to the relative dispersion. It grows respectively as D^2 and $D^{4/3}$ for distances smaller or larger than roughly 10 km. The similarity of the coherent structures in the western Mediterranean basin to those in two dimensional turbulence, and the similar laws of relative dispersion and relative diffusivity, support the existence of the enstrophy and inverse energy cascades for the upper western Mediterranean Sea dynamics.

At 500 m depth, the integral time scale increases and the intermediate regime becomes narrower than the surface one due to weaker effect of vortices (which decreases with depth). The turbulence becomes more homogeneous and the Richardson law takes place.

Further work will investigate the submesoscale dynamics. Indeed, the intense coherent vortices and filaments play a significant role for marine ecosystem in the western Mediterranean Basin. The use of a biogeochemical model coupled with the physical circulation model will allow us to assess the impact of these eddies on biological processes.

References

Babiano, A., Basdevant, C., Leroy, P., and Sadourny, R.: Relative dispersion in two-dimensional turbulence, J. Fluid Mech., 214, 535–557, 1990.

Conkright, M. E., Locarnini, R. A., Garcia, H. E. H.E., O'Brian, T. D., Boyer, T., Stephens, C. and Antonov, J. I.: World Ocean Atlas 2001: Objective Analyses, Data Statistics, and Figures,

OSD

10, 1099–1125, 2013

CD-ROM Documentation 2001, National Oceanographic Data Center, Silver Spring, MD, 17, 2002.
Da Silva, A. M., Young, C. C., and Levitus, S.: Atlas of surface marine data. Algorithms and procedures. NOAA Atlas NESDIS 6. U.S. Department of Commerce, NOAA, NESDIS. Volume 1, 1994.
Elhmaidi, D., Provenzale, A., and Babiano, A.: Elementary topology of the two-dimensional turbulence from a Lagrangian viewpoint and single particle dispersion, J. Fluid Mech., 257, 533-558, 1993.
Elhmaidi, D., Hardenberg, J. V., and Provenzale, A.: Large-scale dissipation and filament instability in two-dimensional turbulence, Phys. Rev. Lett., 95, 1–4, 014503, doi:10.1103, 2005.
Elhmaidi, D., Nefzi, H., Carton, X., and Lili, T.: Particle dispersion in the western Mediterranean Basin, The Open Oceanography Journal (TOOJ), 4, 137–143, 2010.
Haidvogel, D. B., Arango, H. G., and Hedstrom, K.: Model evaluation experiments in the north atlantic basin: simulations in nonlinear terrain-following coordinates, Dynam. Atmos. Oceans, 32, 239–81, 2000.
LaCasce, J. H. and Bower, A.: Relative dispersion in the subsurface North Atlantic, J. Mar. Res., 58, 863–894, 2000.
LaCasce, J. H. and Ohlmann, J. C.: Relative dispersion at the surface of the Gulf of Mexico, J. Mar. Res., 61, 285–312, 2003.
Lumpkin, R. and Elipot, S.: Surface drifter pair spreading in the North Atlantic, J. Geophys. Res., 115,1-20, C12017, doi:10.1029/2010JC006338, 2010.
Marchesiello, P., McWilliams, J. C., and Shchepetkin, A.: Open boundary condition for long-term integration of regional oceanic models, Ocean Model., 3, 1–21, 2001.
Millot, C.: Circulation in the western Mediterranean Sea, Journal of Marine Systems, 20, 423–442, 1999.
Millot, C. and Taupier-Letage, I.: Additional evidence of LIW entrainment across the Algerian Basin by mesoscale eddies and not by a permanent westward flow, Prog. Oceanogr., 66, 231–50, 2005.
Ollitrault, M., Gabillet, C., and Colin De Verdière, A.: Open ocean regimes of relative dispersion, J. Fluid Mech., 533, 381–407, 2005.
Penven, P., Cambon, G., Tan, T., Marchesiello, P., and Debreu, L.: http://www.romsagrif.org/index.php/documentation, 2010.

OSD
10, 1099–1125, 2013

Penven, P., Marchesiello, P., Debreu, L., and Lefèvre, J.: Software tools for pre- and post processing of oceanic regional simulations, Environ. Model. Softw., 23, 660–662, 2008.
Richardson, L. F.: Atmospheric diffusion shown on a distance-neighbor graph, P. Roy. Soc. A, 110, 709–737, 1926.
Shchepetkin, A. F. and McWilliams, J. C.: The regional oceanic modeling system (ROMS): a split-explicit, free-surface, topography following – coordinate oceanic model, Ocean Model., 9, 347–404, 2005.
Smith, W. H. F. and Sandwell, D. T.: Global sea floor topography from satellite altimetry and ship depth soundings, Science, 227, 1956–62. 1997.
Song, Y. and Haidvogel, D. B.: A semi-implicit ocean circulation model using a generalized topography-following coordinate system, J. Comp. Physiol., 115, 228–44, 1994.

OSD
10, 1099–1125, 2013

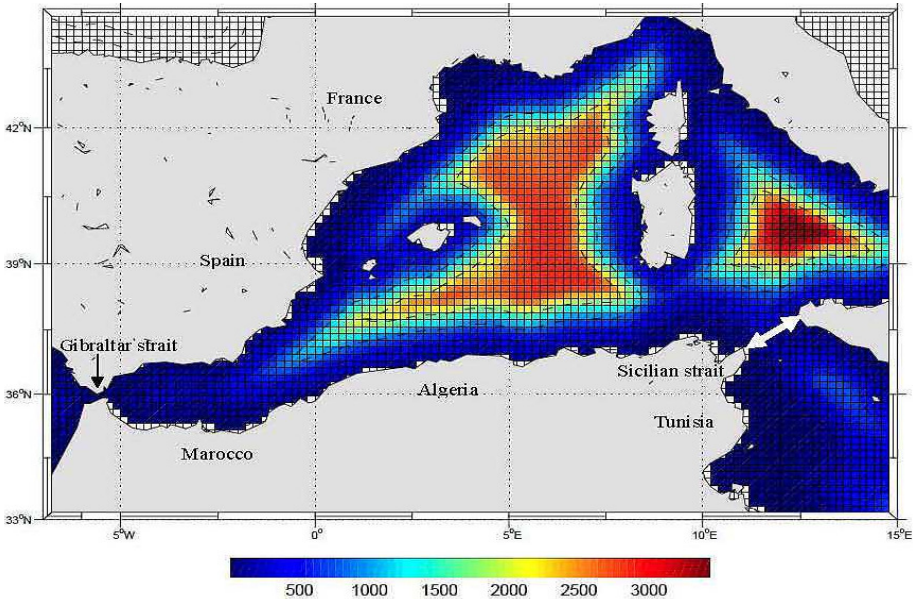

Fig. 1. The model domain and its bathymetry (m).

OSD
10, 1099–1125, 2013

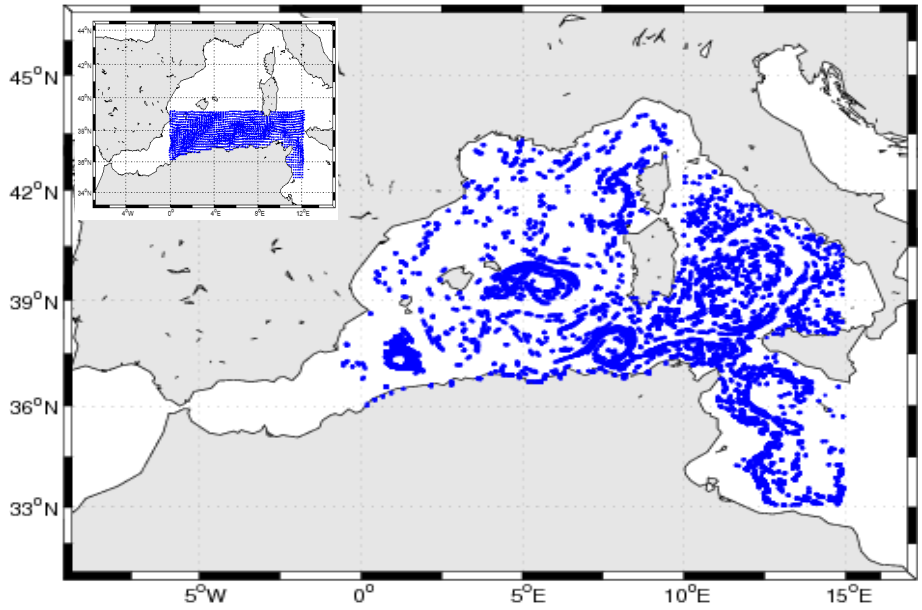

Fig. 2. The particle positions after 2 months of integration. In the inset, we show the initial particle positions.

OSD
10, 1099–1125, 2013

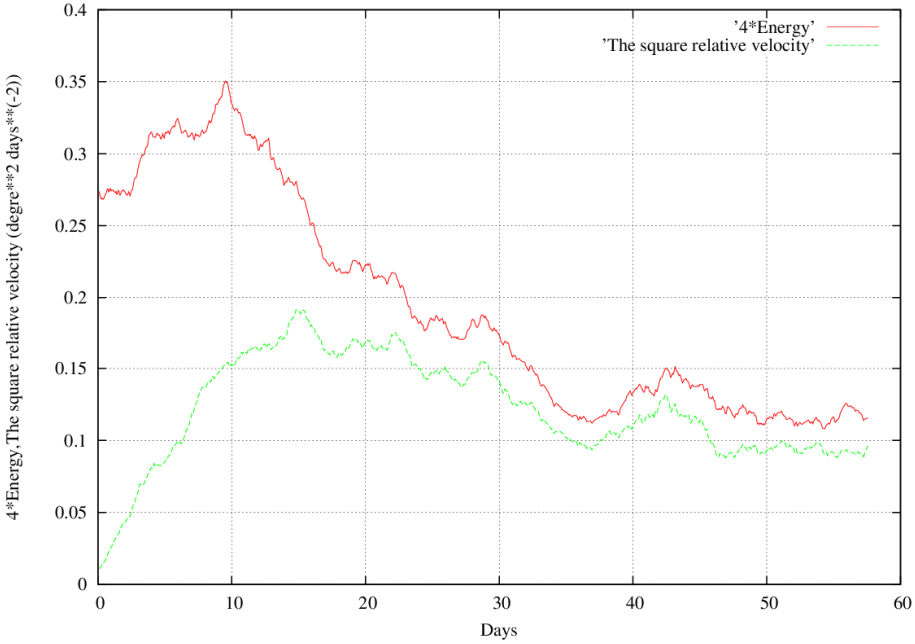

Fig. 3a. Temporal evolution of the mean square relative velocity and the four times the eddy kinetic energy.

OSD
10, 1099–1125, 2013

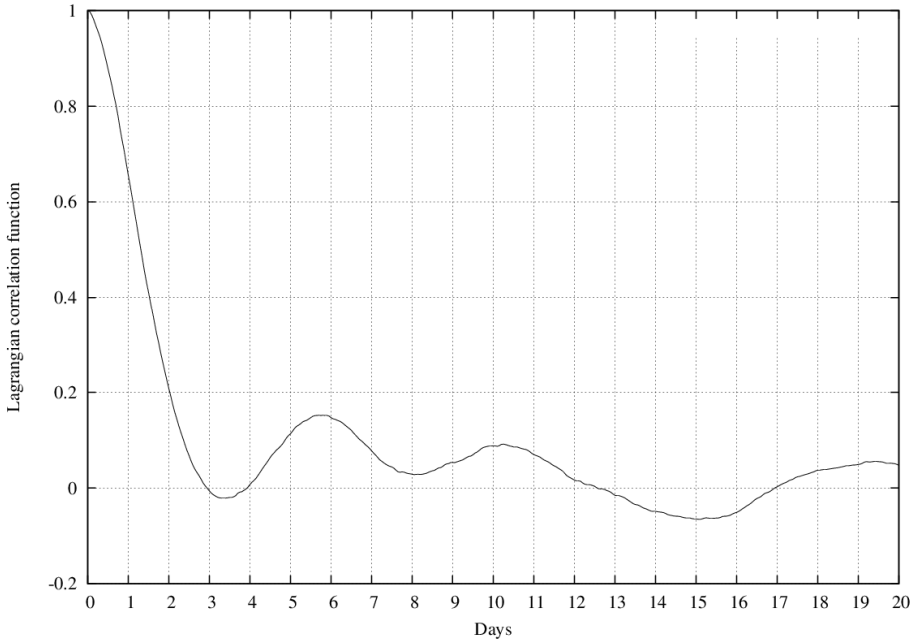

Fig. 3b. Temporal evolution of the 44 m depth lagrangian autocorrelation function.

OSD
10, 1099–1125, 2013

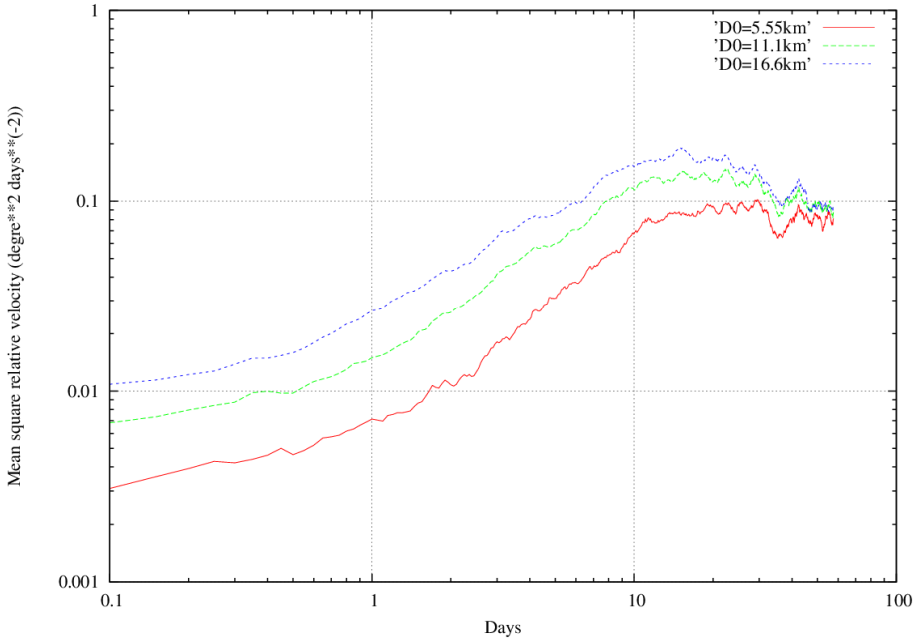

Fig. 3c. Temporal evolution of the zonal mean square relative velocity.

OSD
10, 1099–1125, 2013

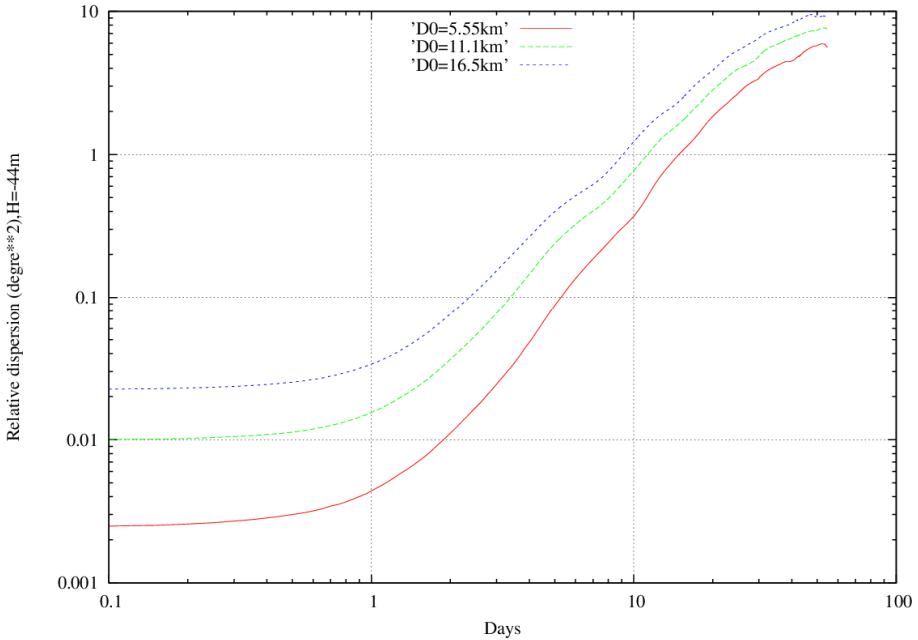

Fig. 4a. The zonal relative dispersion versus time and D_0.

OSD
10, 1099–1125, 2013

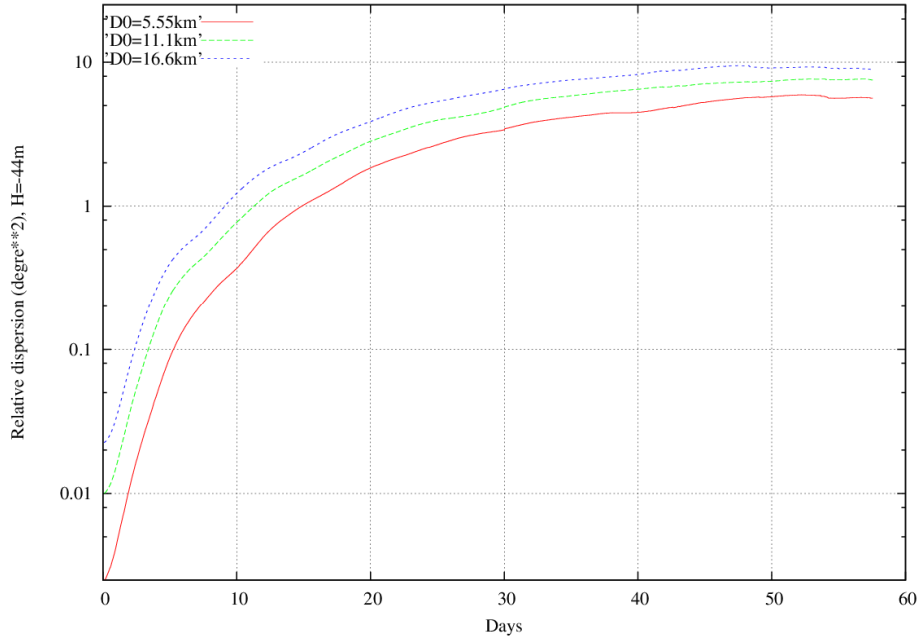

Fig. 4b. The zonal relative dispersion versus time and D_0.

OSD
10, 1099–1125, 2013

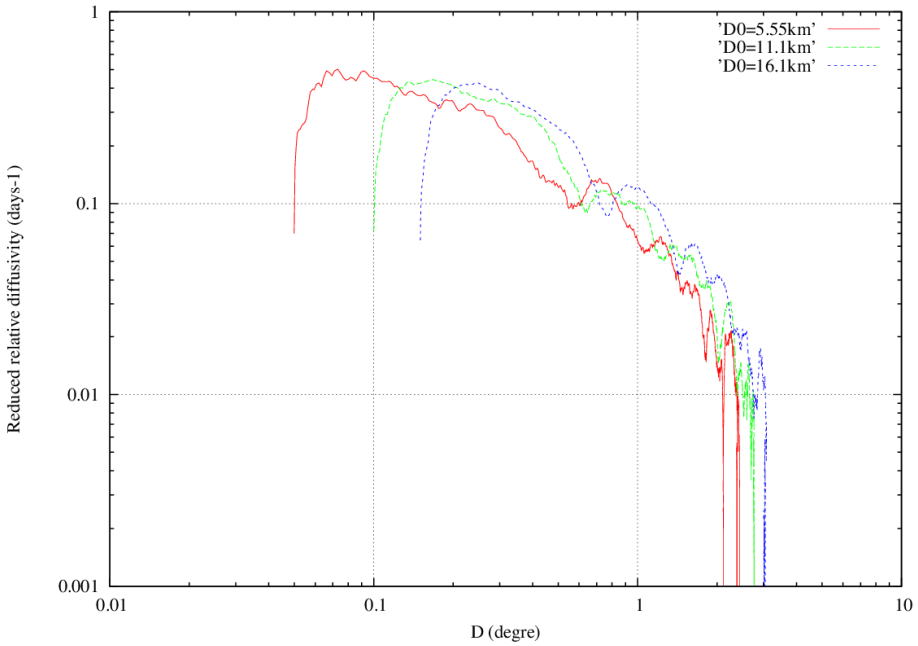

Fig. 5a. The relative diffusivity compensated by $D^{(-2)}$ as function of D.

OSD
10, 1099–1125, 2013

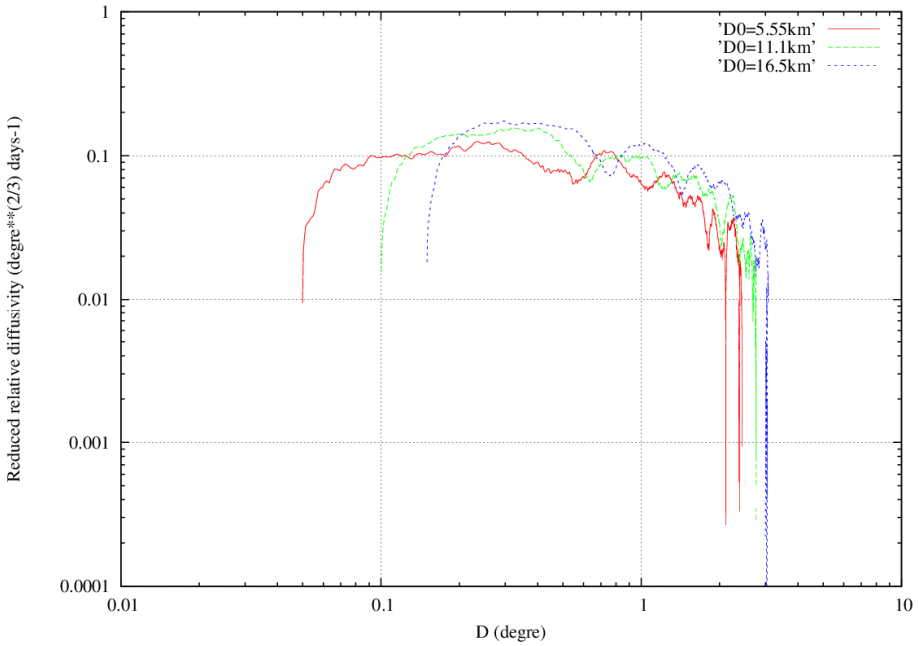

Fig. 5b. The relative diffusivity compensated by $D^{(-4/3)}$ as function of D.

OSD
10, 1099–1125, 2013

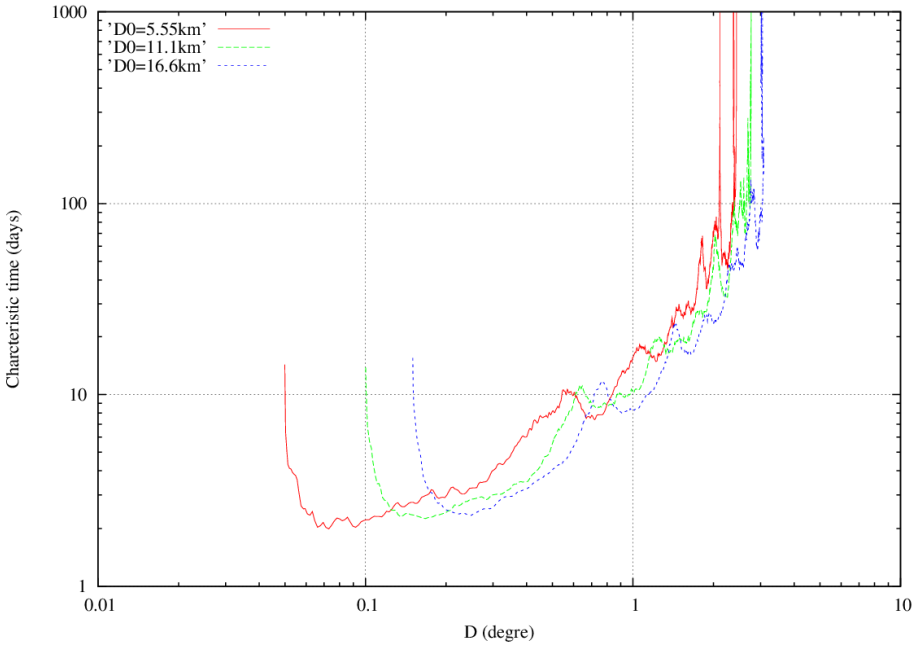

Fig. 6a. The characteristic dispersion time as function of *D*.

OSD
10, 1099–1125, 2013

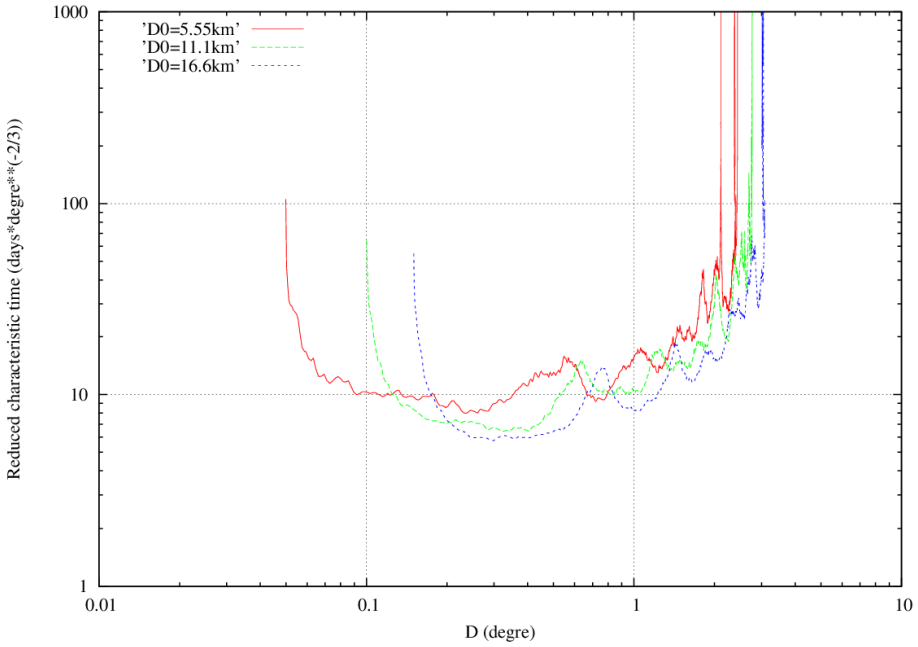

Fig. 6b. The characteristic dispersion time compensated by $D^{(-2/3)}$ as function of D.

OSD
10, 1099–1125, 2013

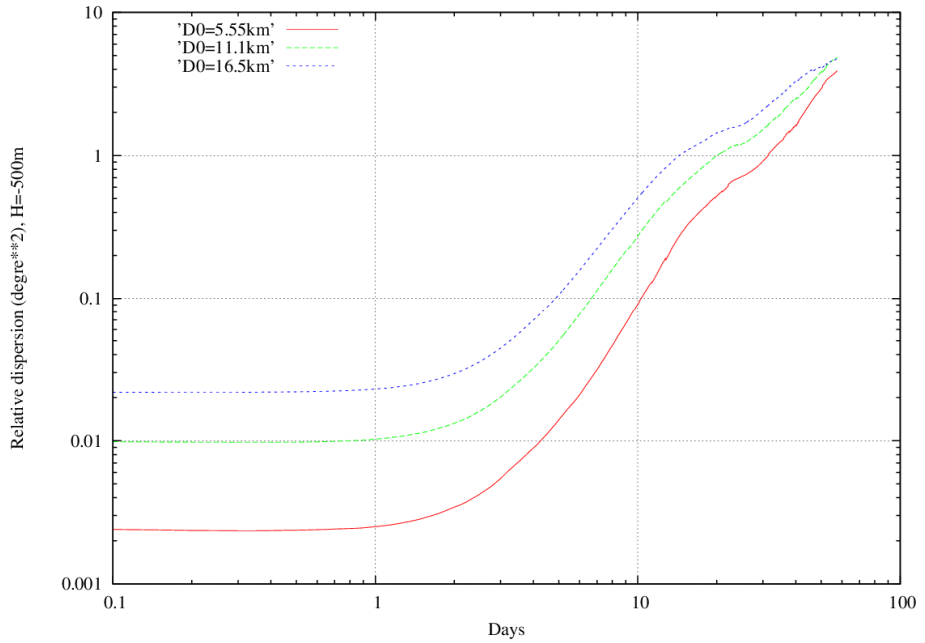

Fig. 7. Temporal evolution of the 500 m depth relative dispersion for different value of D_0.

OSD
10, 1099–1125, 2013

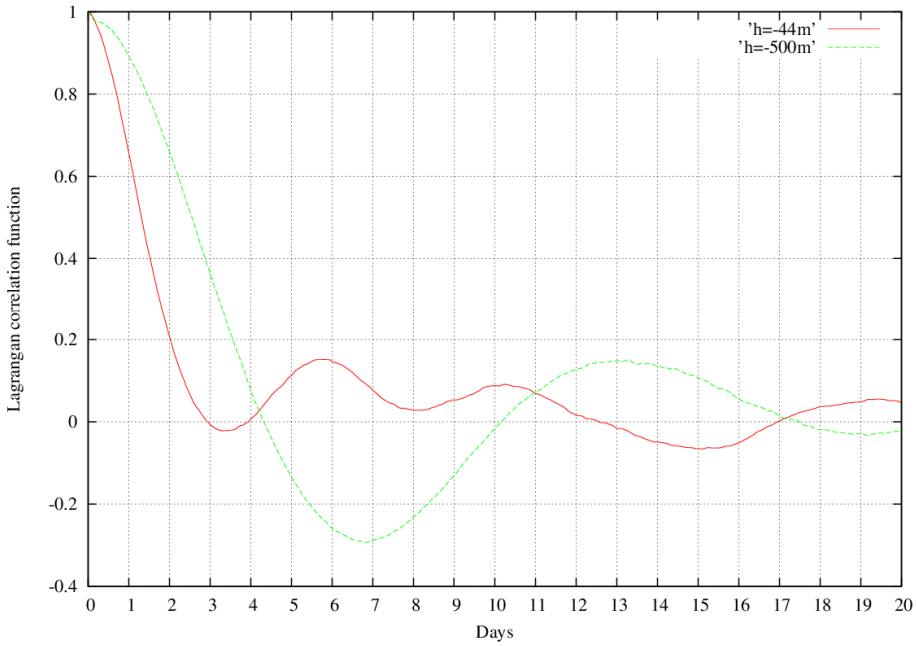

Fig. 8. Temporal evolution of the Lagrangian correlation function at depths 44 and 500 m.

OSD
10, 1099–1125, 2013

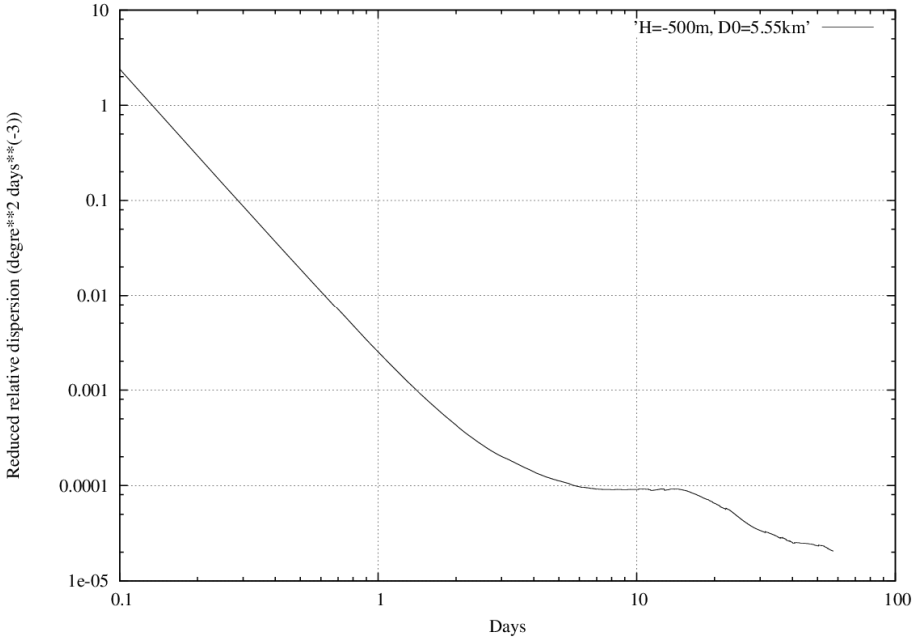

Fig. 9. The 500 m depth relative dispersion compensated by $t^{(-3)}$ for D_0 = 5.55 km.

OSD
10, 1099–1125, 2013